

HMD-EgoPose: Head-Mounted Display-Based Egocentric Marker-Less Tool and Hand Pose Estimation for Augmented Surgical Guidance

Mitchell Doughty^{1,2} and Nilesh R. Ghugre^{1,2,3}

¹ Department of Medical Biophysics, University of Toronto, Toronto, Canada

² Schulich Heart Program, Sunnybrook Health Sciences Centre, Toronto, Canada

³ Physical Sciences Platform, Sunnybrook Research Institute, Toronto, Canada
mitchell.doughty@mail.utoronto.ca

Abstract. Purpose: The success or failure of modern computer-assisted surgery procedures hinges on the precise six-degree-of-freedom (6DoF) position and orientation (pose) estimation of tracked instruments and tissue. In this paper, we present HMD-EgoPose, a single-shot learning-based approach to hand and object pose estimation and demonstrate state-of-the-art performance on a benchmark dataset for monocular red-green-blue (RGB) 6DoF marker-less hand and surgical instrument pose tracking. Further, we reveal the capacity of our HMD-EgoPose framework for 6DoF near real-time pose estimation on a commercially available optical see-through head-mounted display (OST-HMD) through a low-latency streaming approach.

Methods: Our framework utilized an efficient convolutional neural network (CNN) backbone for multi-scale feature extraction and a set of subnetworks to jointly learn the 6DoF pose representation of the rigid surgical drill instrument and the grasping orientation of the hand of a user. To make our approach accessible to a commercially available OST-HMD, the Microsoft HoloLens 2, we created a pipeline for low-latency video and data communication with a high-performance computing workstation capable of optimized network inference.

Results: HMD-EgoPose outperformed current state-of-the-art approaches on a benchmark dataset for surgical tool pose estimation, achieving an average tool 3D vertex error of 11.0 mm on real data and furthering the progress towards a clinically viable marker-free tracking strategy. Through our low-latency streaming approach, we achieved a round trip latency of 202.5 ms for pose estimation and augmented visualization of the tracked model when integrated with the OST-HMD.

Conclusion: Our single-shot learned approach, which optimized 6DoF pose based on the joint interaction between the hand of a user and a rigid surgical drill, was robust to occlusion and complex surfaces and improved on current state-of-the-art approaches to marker-less tool and hand pose estimation. Further, we presented the feasibility of our approach for near real-time tracking on a commercially available OST-HMD.

Keywords: Single-shot pose estimation, marker-less, registration, deep learning, head-mounted displays.

1 Introduction

In their 1994 paper, Milgram and Kishino have detailed a continuum to describe how virtual and real environments can be combined to create different experiences for a user [1]. Augmented reality (AR) systems, encompassing real-world and virtual elements, provide the ability to combine, register, and display interactive 3D virtual content in real-time. Head-mounted displays (HMD), hand-held, and spatial display systems have been proposed for visualization of virtually augmented content [2].

Augmented reality has been described as a potentially disruptive technology in the medical field due to its ability to enhance task localization and accuracy when effectively implemented [3]. To better guide users to target structures, a necessary condition in AR-based navigation is the ability to precisely align, and maintain alignment of, three-dimensional (3D) virtual models with real-world objects [4]. In the context of state-of-the-art surgical navigation systems, continuous and precise intraoperative localization of surgical tools with respect to the patient anatomy is essential to the success of a procedure and safety of the patient [5]. Recent work has highlighted the potential benefits of optical see-through head-mounted displays (OST-HMDs) as the visualization medium for leading surgical navigation, as opposed to the typical monitor-led display of commercial surgical navigation suites [6]. Unlike traditional navigation suites, optical see-through HMDs provide the capacity to eliminate the visual disconnect present between the information presented on a monitor and the surgical scene [7]–[9] and, using context-aware predictions from egocentric video, ensure that the current virtual augmentation meets the current information needs of the user [10].

Though recent work has indicated the applicability of AR for leading surgical navigation in laparoscopic and endoscopic procedures [11], neurosurgery [12], orthopedic surgery [13], targeted cardiac procedures [14], and general surgery [15], there remains the concern of inconsistent intraprocedural instrument position and orientation (pose) estimation, contributing to failed registration and tracking, and the potential for poor surgical outcomes [16].

1.1 Motivation

Several different techniques for surgical instrument localization have been investigated including electromagnetic tracking [17], optical tracking [18] and image-based tracking [19]. Within a specified working volume, commercial infrared optical tracking systems are capable of sub-millimeter tracking accuracy of surgical tools at a high update rate using a 3D stereo matching approach [18]; however, consistent pose measurements rely on an extensive pre-procedural calibration procedure and direct and uninterrupted intraprocedural line-of-sight between the optical markers and imaging sensor [5]. Similar occlusion-based limitations exist with two-dimensional (2D) marker-based tracking techniques which make use of red-green-blue (RGB) camera data and planar fiducial markers to predict pose based on a 2D feature matching strategy [20]. Electromagnetic systems bypass the direct line of sight requirement of image-based tracking systems but require significant setup time, provide a relatively small tracking volume, and tracking accuracy is sensitive to the presence of metal in the workspace [21].

In recent years, deep learning has contributed to the improved interpretation of complex high-dimensional data and has established its position as the state-of-the-art approach in many different computer vision-based tasks including image classification [22], object detection [23], and six-degree-of-freedom (6DoF) object pose estimation [24]. In contrast to prior line-of-sight tracking strategies, a data-driven approach to 6DoF object pose estimation can be less sensitive to scene clutter and occlusion and does not require the precise placement of fiducial markers and additional system calibration for accurate tracking [25].

1.2 Related work

Marker-free object pose estimation remains a challenging and important problem in the context of computer vision and AR. There is a substantial (and rapidly growing) body of research work with proposed solutions to the problem of 6DoF object pose recovery; prior strategies have included template-based [26], point-to-point [27], conventional learning-based [28], [29], and deep learning-based techniques [25].

Deep learning-led techniques are the current best-performing approaches in the 6DoF object pose estimation space and leverage large amounts of high-quality curated data to learn deep discriminative feature representations [25]. The majority of deep learning-based hand and object pose estimation techniques have relied on depth information or used red-green-blue-depth (RGB-D) camera frames for prediction [29]–[33]. For our intended use case for tool tracking during surgical interventions, the close proximity of tracking targets and challenging lighting conditions in the operating room present significant challenges in the effective use of RGB-D data [34]. In this work, we focused on addressing the challenging problem of estimating hand and object pose from monocular RGB video.

Object pose estimation. We can broadly categorize the deep learning-based 6DoF object pose estimation from monocular RGB literature into single-shot and iterative refinement approaches. Single-shot strategies have used a convolutional neural network (CNN) to predict 6DoF object pose directly without requiring multiple stages or hypothesis [24], [35]–[37]. Iterative refinement techniques have used a CNN to first predict the 2D locations of the 3D bounding boxes which define an object in image space, then obtain the 6DoF object pose via perspective-n-point (PnP) or additional iterative refinement like random sample consensus (RANSAC) [38]–[43]. Due to their indirect pose estimation approach, iterative refinement-based techniques typically report slower inference times and require more computational power than single-shot approaches [36].

Hand pose estimation. Prior approaches to hand pose estimation from monocular RGB data have focused on reducing the complexity of the problem by using a set of predefined hand poses [44] or simplified hand representations [45]. As with object pose estimation, deep learning-based strategies have pushed the current state-of-the-art performance of hand pose estimation techniques [46]. Several strategies have focused on

directly regressing the 3D skeleton joint positions from RGB input frames [47]–[50], where others have used parametric hand models with shape and pose parameters to describe 3D hand mesh representations [51], [52].

Joint hand and object pose estimation. The joint prediction of hand and object poses has the capacity to offer a rich understanding of how users interact with objects in their environment. Due to the nature of hand-object interactions, there are large mutual occlusions which occur during object handling and manipulation, making accurate pose estimation a difficult problem [53]. In recent work, Hasson et al. build off of the parametric hand model, MANO [51], and use a CNN-based approach (HandObjectNet) to leverage constraints imposed by typical hand-object interactions and reconstruct hand and object pose from monocular RGB video [53], [54]. Related to the surgical domain, Hein et al. recorded a monocular RGB-based benchmark dataset of hand and surgical tool interactions and investigated the performance and feasibility of different learned approaches to joint hand and object pose estimation [34].

1.3 Objectives

Our goals were (1) to design a single-shot network which improved on the accuracy and speed of prior 6DoF rigid object and hand pose estimation techniques using monocular RGB data; and (2) to demonstrate the feasibility of an OST-HMD led tracking experience using a streaming approach with egocentric video captured from the headset.

With HMD-EgoPose, we demonstrated state-of-the-art performance on a benchmark dataset for surgical drill and hand pose estimation. Further, we revealed the feasibility of a low-latency streaming approach to send egocentric monocular RGB data to a high-performance computing workstation for optimized inference and enable 6DoF pose estimation on a commercially available OST-HMD. Our code is publicly available at <https://github.com/doughtmw/hmd-ego-pose>.

2 Materials and Methods

To jointly model the interactions between a surgical tool and the hand of a user, we build our network based on the EfficientDet [55] backbone for multi-scale feature extraction and took influence from the EfficientPose [36] architecture to introduce several subnetworks, which achieved the goal towards lightweight single-shot 6DoF hand and tool pose estimation (Figure 1).

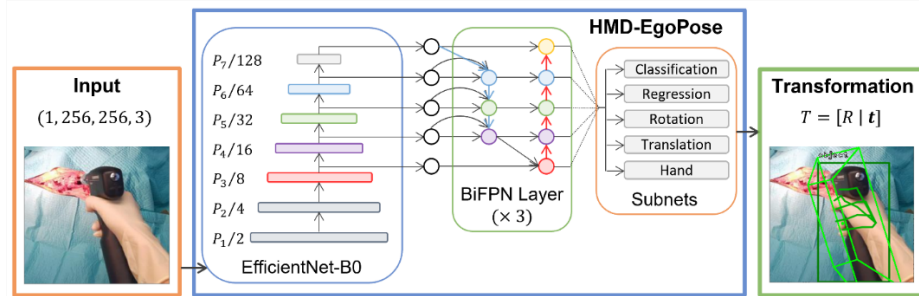


Fig. 1. Overview of HMD-EgoPose, the single-shot deep learning-based framework for the prediction of relevant information regarding the joint hand and surgical tool interaction from a single monocular red-green-blue (RGB) input image frame. We made use of the EfficientNet [56] backbone and the weighted bi-directional feature pyramid network (BiFPN) from the EfficientDet [55] architecture alongside a set of additional subnets. Using our approach, we classified the tool in frame, regressed a two-dimensional (2D) bounding box around the object, estimated a rotation and translation component to describe the six-degree-of-freedom (6DoF) pose of the rigid surgical tool, and estimated the three-dimensional (3D) vertex parameters to describe the pose of the hand.

2.1 Joint hand and tool estimation

Using a CNN-based approach, we proposed HMD-EgoPose, an architecture for 6DoF rigid object and hand pose estimation based on learned deep discriminative features about joint hand-and-tool interactions. Our method takes as input monocular RGB video from an egocentric point of view that captures the hands of a surgeon interacting with a rigid surgical tool and provides an estimate of 6DoF pose of the surgical tool in frame and the 3D skeleton positions of hands.

Multiscale feature fusion. To address scaling issues common to CNNs, Tan and Le have proposed the EfficientNet framework, generated from a compound scaling method which uniformly scales the network width, depth, and resolution based on a fixed set of scaling coefficients [56]. Building off of the EfficientNet backbone, Tan et al. introduced EfficientDet, a network which incorporated a weighted bi-directional feature pyramid network (BiFPN) for multi-scale feature fusion to effectively represent and process multi-scale features for object detection [55]. To extend the state-of-the-art 2D object detection performance of EfficientDet into our 3D task, we took influence from the EfficientPose [36] architecture and introduced a series of subnetworks to estimate the 3D vertex positions of the hands of a user and 6DoF transformation (rotation and translation) describing the pose of the object in frame.

Rotation network. We based our rotation subnetwork off of the classification and box network used in the EfficientDet [55] architecture. Our rotation subnetwork used an axis-angle representation and directly regressed a rotation vector ($\mathbf{r} \in SO(3)$) from convolutional features extracted within each anchor box. To train our rotation

subnetwork for axis-angle rotation prediction, we used the average squared distance between points of the correct model pose (\mathbf{r}) and their corresponding predictions ($\tilde{\mathbf{r}}$) [24]. We defined our rotation loss as:

$$RLoss(\tilde{\mathbf{r}}, \mathbf{r}) = \frac{1}{2m} \sum_{x \in M} \|\tilde{\mathbf{r}}x - \mathbf{r}x\|^2 \quad (1)$$

where M is the set of 3D model points, m is the number of points in the set, \mathbf{r} denotes the axis-angle rotation for the ground truth pose, and $\tilde{\mathbf{r}}$ indicates the axis-angle rotation for the predicted pose.

Translation network. Like with the rotation subnetwork, we based our translation subnetwork off of the classification and box network used in the EfficientDet [55] architecture. Taking influence from PoseCNN [24], our translation subnetwork regressed a 2D object center point $\mathbf{c} = (c_x, c_y)^T$ in pixel coordinates and a translation distance component t_z , separately, from convolutional features extracted within each anchor box. A translation vector ($\mathbf{t} \in \mathbb{R}^3$) for the object was then composed using the object center point \mathbf{c} , the distance component t_z , and knowledge of the camera intrinsic parameters. The missing translation components, t_x and t_y were computed as follows:

$$t_x = \frac{(c_x - p_x) \cdot t_z}{f_x} \quad (2)$$

$$t_y = \frac{(c_y - p_y) \cdot t_z}{f_y} \quad (3)$$

where the principal point $\mathbf{p} = (p_x, p_y)^T$ and focal lengths f_x, f_y were derived from the camera intrinsic parameters. We modeled our translation loss using the smoothed $L1$ loss between the ground truth translation (\mathbf{t}) and the predicted translation ($\tilde{\mathbf{t}}$) as:

$$TLoss(\tilde{\mathbf{t}}, \mathbf{t}) = \frac{1}{2m} \sum_{x \in M} smooth_{L1}(\tilde{\mathbf{t}}x - \mathbf{t}x) \quad (4)$$

$$smooth_{L1}(x) = \begin{cases} 0.5x^2 & \text{if } |x| < 1 \\ |x| - 0.5 & \text{otherwise} \end{cases} \quad (5)$$

where M is the set of 3D model points, m is the number of points in the set, \mathbf{t} denotes the translation for the ground truth pose, and $\tilde{\mathbf{t}}$ indicates the translation for the predicted pose. The final 6DoF transformation, T , for the predicted object pose was composed of the rotation matrix $R \in \mathbb{R}^{3 \times 3}$, computed from the axis-angle rotation representation \mathbf{r} , and translation components as $T = [R \mid \mathbf{t}] \in \mathbb{R}^{4 \times 4}$.

Hand network. Building off of the ideas introduced in the rotation and translation sub-networks, we based our hand subnetwork off of the classification and box network used in the EfficientDet [55] architecture. Our hand subnetwork used a vector representation to model the 3D skeleton vertices of the hand and directly regressed a vector ($\mathbf{h} \in \mathbb{R}^{3 \times 21}$) from convolutional features extracted from within each anchor box.

To train our hand subnetwork for the prediction of the 3D skeleton vertices of the hand, we used the average squared distance between points of the correct hand skeleton pose (\mathbf{h}) and their corresponding predictions ($\tilde{\mathbf{h}}$) [24]. We defined our hand vertex loss as:

$$HLoss(\tilde{\mathbf{h}}, \mathbf{h}) = \frac{1}{2m} \sum_{x \in M} smooth_{L1}(\tilde{\mathbf{h}}x - \mathbf{h}x) \quad (6)$$

where M is the set of 3D model points, m is the number of points in the set, \mathbf{h} denotes the ground truth hand vertex vector, and $\tilde{\mathbf{h}}$ indicates the predicted hand vertex vector.

2.2 Datasets

We used the synthetic and real datasets presented by Hein, et al [34] for benchmarking the performance of HMD-EgoPose. Both datasets used the Colibri II battery powered orthopedic drill (DePuy Synthes, Raynham, MA, U.S) for rigid tool tracking and incorporated hand information while grasping the instrument. Images were annotated with the 6DoF tool pose of the instrument in frame and the 3D hand joints of the user grasping the tool.

Synthetic Colibri dataset. The synthetic Colibri (SynColibri) dataset included a total of 10,500 image frames (256×256 pixel resolution), created through a detailed synthetic data generation pipeline [34]. SynColibri contains an accurate 3D surgical drill model, a set of 7 possible tool-specific grasp poses for the drill, a human body model, realistic surgical lighting conditions and background, and a hand texture that resembles that of surgical gloves; more details on the data generation pipeline are available from the authors [34]. During synthetic data generation, the distance between the virtual camera and 3D drill model was uniformly selected between 30 cm to 50 cm.

Our framework was implemented using the PyTorch [57] deep learning library. We trained our network on the SynColibri dataset for 500 epochs with a batch size of 32. For all experiments, we used a computing workstation with an AMD Ryzen 9 3900X CPU and a single NVIDIA RTX 3090 GPU with 24 GB GDDR6X memory. For optimization on the SynColibri dataset, we used the Adam [58] optimizer and an initial learning rate of $1e^{-4}$. During training on both the SynColibri and real Colibri (RealColibri) datasets, we performed extensive 6D augmentation of input data including random rotations, scaling, and translations as well as color space augmentation like adjusting contrast and brightness [36]. For both the SynColibri and RealColibri dataset,

we replicated the same five-fold cross-validation strategy as in [34] to assess variance across data splits and ensure our results are directly comparable to benchmarks.

Real Colibri dataset. The RealColibri dataset included a total of 3,746 frames (256×256 pixel resolution) extracted from a total of 11 individual recordings and captured through use of a mock operating room and human cadaveric specimen with an open incision [34]. Two users were asked to assist in handling of the Colibri II surgical drill during data collection and were instructed to wear different colored pairs of rubber gloves. During real data generation, the distance between the camera and the 3D drill model varied based on the comfort and arm-length of the user but is expected to be within a similar 30 cm – 50 cm distance as with the SynColibri dataset.

We fine-tuned our network on the RealColibri dataset, using the best performing weights from network training on the SynColibri dataset, for 500 epochs with a batch size of 32. For optimization on the RealColibri dataset, we used stochastic gradient descent (SGD) with a momentum of 0.9 and a reduced learning rate of $1e^{-5}$.

2.3 Evaluation metrics

As our primary focus was with regards to the assessment of tool tracking accuracy, we measured the mean 3D errors of our predicted rigid surgical drill pose relative to the ground truth pose (ADD_{tool}) and provided assessments of positional error (in mm) and rotational error (in degrees) at the tip of the 3D drill model. We defined our measure of mean 3D errors of surgical drill pose as:

$$ADD_{tool} = \frac{1}{m} \sum_x \|(R\mathbf{x} + \mathbf{t}) - (\tilde{R}\mathbf{x} + \tilde{\mathbf{t}})\| \quad (7)$$

Where m is the number of points in the 3D model set, R and \tilde{R} are the ground truth and predicted rotation matrices, respectively, \mathbf{t} and $\tilde{\mathbf{t}}$ are the ground truth and predicted translation vectors, and x represents the 3D model points of the rigid surgical drill model set. Additionally, we assessed the performance of our 3D hand vertex predictions by computing the mean end-point error across the 21 predicted joints (ADD_{hand}) [34], [54]. We described our measure of hand vertex error as:

$$ADD_{hand} = \frac{1}{m} \sum_x \|\mathbf{h} - \tilde{\mathbf{h}}\| \quad (8)$$

where m is the number of points in the 3D set, and \mathbf{h} and $\tilde{\mathbf{h}}$ are the ground truth and predicted hand vertex vectors, respectively. To evaluate the runtime performance of our network, we included an estimate of the total number of parameters in each model, the model size, the FLOPS for an input image of size (1, 3, 256, 256), and the inference time (latency) measured using a single NVIDIA RTX 3090 GPU and a batch size of 1 across 1000 samples of the testing data.

2.4 Low-latency streaming for head-mounted display-led pose estimation

We used the Microsoft HoloLens 2 (<https://www.microsoft.com/en-us/hololens>, accessed on 23 February 2022) OST-HMD to record egocentric video frames and display 6DoF pose estimations of the tracked surgical drill as an augmented 3D virtual model. The headset features several cameras, including visible light environment tracking cameras, a short and long throw depth camera, and an autofocus photo-video RGB camera. Two 2D laser beam scanning displays are used to display 3D virtual models via stereoscopic vision to the wearer with a field of view of 43×29 degrees (horizontal \times vertical). To estimate the required intrinsic parameters for computing 6DoF object pose, we performed a standard camera calibration procedure of the RGB photo-video camera sensor (896×504 pixels). Intrinsic parameters including focal length (f_x, f_y), principal points (p_x, p_y), and skew (s) were computed to describe perspective projection to relate 3D points in the camera coordinate frame to their 2D image projections [59].

Video streaming from head-mounted display to desktop. To drive our pose estimation framework, we requested egocentric input video frames of size 896×504 pixels from the HoloLens 2 photo-video RGB camera at 30 frames per second (FPS). We built our application using the Unity C# development platform (<https://unity.com/>, accessed on 23 February 2022) and implemented our real-time video and data communication protocol using the WebRTC library (<https://github.com/microsoft/MixedReality-WebRTC>, accessed on 23 February 2022) to enable low-latency communication with our remote desktop peer. With a WebRTC C++ dynamic link library (DLL), we used the universal datagram protocol (UDP) and an H.264 codec for streaming video frames in a compressed YUV420 representation from the HoloLens 2 to our high-performance computing workstation (Figure 2).

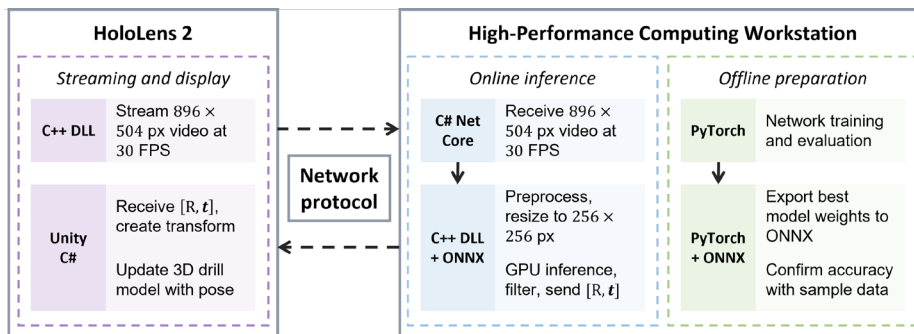


Fig. 2. Overview of the streaming approach for head-mounted display-led pose estimation via low-latency streaming of video frames from the HoloLens 2 to a computing workstation equipped for optimized network inference. We also included the steps used for offline preparation of the network and trained model weights. Video frames are sent from the HoloLens 2 device to a computing workstation over a WebRTC based network protocol where GPU-based network inference is performed. The six-degree-of-freedom (6DoF) pose estimate of the surgical drill in frame is then returned to the HoloLens 2 and used to track the instrument in the user-centric view.

Optimized inference on a computing workstation. The high-performance computing workstation included a WebRTC C# Net Core project to receive and unpack the incoming YUV420 video frames from the HoloLens 2 to an RGB representation at the original 896×504 pixels and 30 FPS representation. We used a C++ DLL and OpenCV (<https://opencv.org/>, accessed on 23 February 2022) within the C# project for optimal pre-processing of the incoming video frames, including image normalization and bilinear interpolation to a size of 256×256 pixels. For optimal GPU inference, we used the NVIDIA TensorRT software development kit (<https://developer.nvidia.com/tensorrt>, accessed on 23 February 2022) and ONNX library (<https://onnx.ai/>, accessed on 23 February 2022). Following network inference, filtering of the resulting predictions included rescaling, clipping and non-maximum suppression to arrive at a final 6DoF pose prediction result. Using a WebRTC data channel, we sent the resulting axis-angle rotation and translation vectors as a combined 24-byte array to the HoloLens 2 device.

Show pose estimation results on head-mounted display. After receiving and unpacking the incoming byte array with axis-angle rotation and translation components on the HoloLens 2, we formatted the transform for correct representation in the Unity coordinate frame and applied the 6DoF pose to a virtual 3D surgical drill model displayed to the user. We were unable to obtain the exact Colibri II surgical drill used during benchmark dataset collection for qualitative assessment; instead, we 3D printed the Colibri drill file to use as a representative model of the same geometry (3D Printing Canada, Hamilton, ON, Canada). The fused deposition modeling (FDM) printing process was used for 3D printing, resulting in a model with identical geometry but different texture and color than the real drill.

3 Results and Discussion

In this section, we evaluated the performance of HMD-EgoPose relative to current state-of-the-art approaches and assessed the performance and feasibility of 6DoF pose estimation on a commercially available OST-HMD through our low-latency streaming approach and a high-performance computing workstation.

3.1 Experimental results

Hein et al. have presented several strategies for surgical drill and hand pose estimation from monocular RGB data for the synthetic drill dataset based off of the PVNet [39] and HandObjectNet [54] frameworks. PVNet focuses solely on 6DoF object pose estimation and does not consider the joint interaction of the hand of a user with the object [39]. PVNet indirectly estimates object pose using a set of 2D keypoints that correspond to the 3D bounding box center and selected 3D locations across the surface of the model. To estimate a segmentation mask and 2D vector field for each keypoint, PVNet uses a similar architecture as a U-Net [60]. A RANSAC-based voting scheme is used to recover 2D keypoints from their respective 2D vector fields. The final 6DoF tool

pose is recovered using a perspective-n-point (PnP) approach to minimize the Mahalanobis distance based on the mean and covariance of the keypoint predictions and the ground truth keypoints. Instead of solely focusing on 6DoF object pose alone, HandObjectNet considers the joint interaction of the hands of a user and the surgical drill [34]. HandObjectNet uses a shared ResNet-18 [61] encoder and decoders for both the hand and object [54]. The hand decoder branch estimates 18 pose parameters, consisting of 15 coefficients to describe the hand configuration and 3 parameters to detail the axis-angle representation of the hand, and 10 shape parameters to describe the MANO hand model [51]. The object branch regresses an axis-angle rotation vector, 2D translation vector, and a focal-normalized depth offset; the 3D translation is then composed using knowledge of the camera intrinsic parameters [54].

Table 1 compares the performance and latency of our approach relative to other state-of-the-art techniques on the SynColibri surgical drill dataset. Our HMD-EgoPose framework outperformed the HandObjectNet [34], [54] and PVNet [34], [39] techniques in measures of tool ADD and rotational error at the drill bit tip. Our approach used $3\times$ fewer network parameters, required $3\times$ less memory for deployment, achieved $3\times$ faster FLOPS, and required less time for inference than HandObjectNet, the previous best performing approach. Across the synthetic dataset, we achieved an average tool 3D vertex (ADD_{tool}) accuracy of 11.17 mm. Figure 3 includes a sample image frame from the SynColibri dataset with corresponding network predictions for 3D hand vertices and 6DoF rigid surgical drill pose as compared to the ground truth labels.

Table 1. Networks trained and evaluated on the synthetic Colibri surgical drill dataset (mean \pm standard deviation).

	HMD-EgoPose	HandObjectNet [34]	PVNet [34]
Tool ADD (mm)	11.17 \pm 9.17	16.73 \pm 16.97	20.59 \pm 52.14
Drill Tip Error (mm)	34.81 \pm 36.01	44.45 \pm 59.72	31.10 \pm 67.18
Drill Bit Dir Error (deg)	5.40 \pm 6.98	6.59 \pm 10.18	7.11 \pm 21.78
Hand ADD (mm)	19.79 \pm 7.72	17.15 \pm 10.58	–
Network Parameters (M)	3.92	12.49	12.96
Network Size (MB)	16.3	53.1	51.92
FLOPS (B)	1.38	4.76	30.96
Latency (ms)	19.8 \pm 2.3	21.5 \pm 3.3	52.4 \pm 8.2

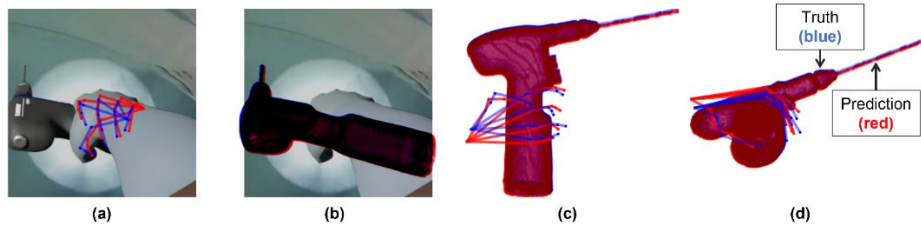


Fig. 3. Sample three-dimensional (3D) hand vertex and six-degree-of-freedom (6DoF) object pose estimates are shown relative to ground truth labels for an image sample from the synthetic Colibri dataset. Predicted labels for hand vertices and model pose are shown in red, and ground truth labels for hand vertices and model pose are in blue. The 2D projections of 3D hand vertices (a) and 2D projections of 3D model points (b) are shown on the related input image frame. A view from the top (c) and the right (d) are included to show the 3D model and hand vertex prediction agreement from different view perspectives.

Table 2 describes the performance and latency of our approach relative to other state-of-the-art techniques on the RealColibri surgical drill dataset. Our HMD-EgoPose framework outperformed the HandObjectNet [34] and PVNet [34] techniques in measures of tool ADD and rotational and translational error at the drill bit tip. Across the real dataset, we achieved an average tool 3D vertex (ADD_{tool}) accuracy of 11.00 mm. Figure 4 shows a sample image frame from the real Colibri dataset with corresponding network predictions for 3D hand vertices and 6DoF rigid surgical drill pose as compared to the ground truth labels. Even with significant mutual occlusion of the hand of a user and the surgical drill, there was good agreement between the 6DoF tool pose and the ground truth information due to the jointly learned hand and tool representation of HMD-EgoPose.

Table 2. Networks pretrained on synthetic data and finetuned and evaluated on real Colibri surgical drill dataset (mean \pm standard deviation).

	HMD-EgoPose	HandObjectNet [34]	PVNet [34]
Tool ADD (mm)	11.00 \pm 7.27	13.78 \pm 5.28	39.72 \pm 66.49
Drill Tip Error (mm)	28.07 \pm 19.81	66.11 \pm 26.91	72.80 \pm 105.66
Drill Bit Dir Error (deg)	3.89 \pm 2.74	8.71 \pm 3.98	13.41 \pm 33.78
Hand ADD (mm)	17.35 \pm 8.09	9.78 \pm 4.54	–

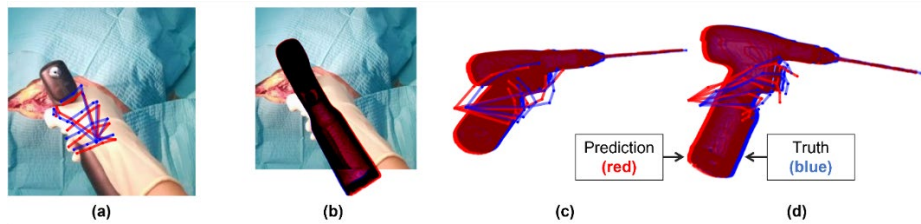


Fig. 4. Sample three-dimensional (3D) hand vertex and six-degree-of-freedom (6DoF) object pose estimates are shown relative to ground truth labels for an image sample from the real Colibri dataset. Predicted labels for hand vertices and model pose are shown in red, and ground truth labels for hand vertices and model pose are in blue. The 2D projections of 3D hand vertices (a) and 2D projections of 3D model points (b) are shown on the related input image frame. A view from the top (c) and the right (d) are included to show the 3D model and hand vertex prediction agreement from different view perspectives. Notice that there is good agreement of the ground truth and predicted metrics even with significant mutual occlusion of the hand and surgical drill.

In our proposed use for 6DoF pose estimation of tracked tools during a surgical intervention, the most critical performance measure was the accuracy of the surgical instrument. Our HMD-EgoPose approach outperformed PVNet and HandObjectNet in measures of accuracy across the entire tool model and, more importantly, demonstrated improved localization of the surgical drill tip through reduced drill tip error and drill bit direction error. HandObjectNet provided more accurate estimates of hand skeleton prediction; however, as our focus was on surgical drill pose accuracy, we prioritized the relative loss weighting of our translation and rotation subnetworks over the hand prediction subnetwork during network training. Along with improved tool pose prediction accuracy, our HMD-EgoPose network exhibited more consistent pose predictions, even when there was significant mutual occlusion present; likely due to the fusion approach to representing multi-scale features across the image space and the jointly learned representation of objects and hands.

3.2 Feasibility assessment of streaming to head-mounted display

In Figure 5, we include a set of sample images from an experiment where a user was asked to hold the 3D printed surgical drill model and move the drill as if they were replicating the movements typical to its use in an orthopedic procedure. All data recorded for the synthetic and real Colibri benchmark datasets included a user grasping the surgical drill in their right hand; we replicated this setup during our assessment and instructed the user to hold the drill model with their right hand. As indicated in the sample frames, there was good agreement between both the predicted and ground truth surgical drill pose estimates. We assessed the mean 2D registration accuracy between the 3D printed surgical drill model and the 3D virtual model visually by capturing 10 still-frame images and measuring the error at three landmark positions: the drill chuck (where the drill bit attachment would be inserted), the base of the drill handle, and the circle on the top back surface of the drill just above where a user would grasp. We measured the mean 2D Euclidean error at these three landmark positions across the image set as 9.2 ± 4.8 mm (mean \pm standard deviation). Across 25 inference samples, we characterized the average pixel-to-photon latency: the cumulative time required for streaming of egocentric video to our high-performance computing workstation, performing GPU inference, returning the results to the HoloLens 2, and rendering them on-screen, as 202.5 ± 20.4 ms. Of this, roughly 170 ms was required for video frame transmission, 6 ms for frame resizing and rescaling, 12 ms for GPU inference in TensorRT and post prediction filtering, and 14 ms for return transmission of the predicted 6DoF transformation to the HoloLens 2 and rendering of the updated virtual model pose. Additional qualitative videos demonstrating the performance of HMD-EgoPose during network inference are available in the supplementary material.

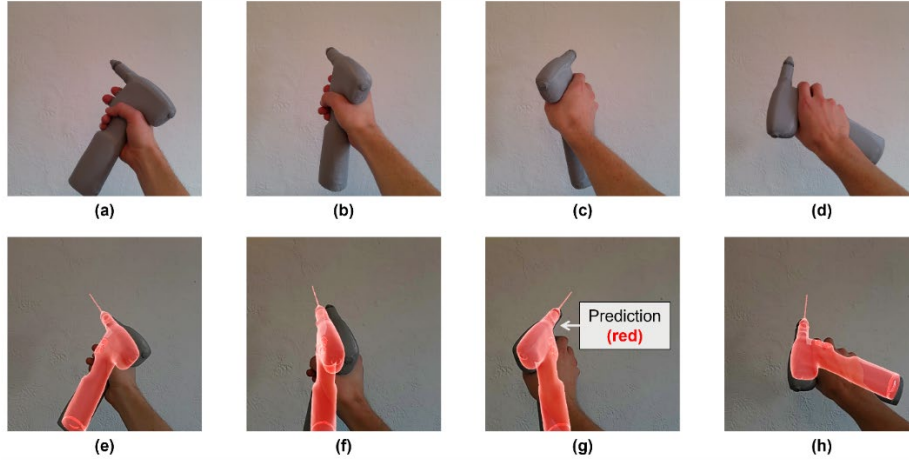


Fig. 5. Sample images demonstrating the real-world tracking accuracy of our network for rigid surgical drill pose estimation on the HoloLens 2 head-mounted display while using a representative three-dimensional (3D) printed model with identical geometry as the Colibri II surgical drill. (a-d) Images captured using the HoloLens 2 photo-video camera prior to launching our tracking application. We include four separate grasping poses of the 3D printed surgical drill model. (e-h) Single frames replicating the grasping poses from images (a-d) captured using the HoloLens 2 mixed reality capture capabilities after launching our tracking application. The two-dimensional (2D) views are created by the mixed reality capture application using the right eye camera of the 3D stereo view on the headset, which is known to introduce an offset in the position of virtual models. Pose predictions from our HMD-EgoPose network are applied to the 3D surgical drill model displayed in red.

3.3 Limitations

Alongside challenges optimal network architecture and training, a primary limitation of learning-based approaches is the quality, size, and diversity of the training dataset. As indicated in Figure 6, there were errors present in some image samples from the RealColibri training dataset due to unstable detection of the surface of the surgical drill by the dual Kinect camera configuration [34]. The unstable detection was caused by reflection errors at the surface of the drill and introduced errors to the point cloud dataset collected, resulting in a degraded ground truth pose estimation computed by iterative closest point (ICP) registration. In future, a data collection setup with additional co-calibrated Kinect cameras could reduce the contribution to error in ground truth pose estimates. Further, we expect that a larger training dataset with multiple users, varying user-handedness, and more complex and diverse surgical backdrops would contribute to improved stability in network performance.

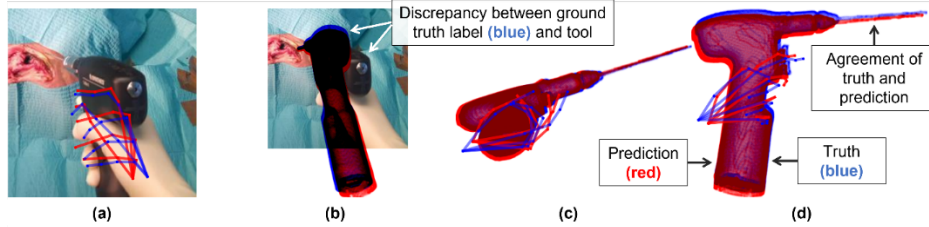


Fig. 6. Sample three-dimensional (3D) hand vertex and six-degree-of-freedom (6DoF) object pose estimates are shown relative to ground truth labels for an image sample from the real Colibri dataset that has experienced significant drift. Predicted labels for hand vertices and model pose are shown in red, and ground truth labels for hand vertices and model pose are in blue. The 2D projections of 3D hand vertices (a) and 2D projections of 3D model points (b) are shown on the related input image frame. In (b) we can also observe the error present between the ground truth tool label (blue) and the actual tool position. A view from the top (c) and the right (d) are included to show the 3D model and hand vertex prediction agreement from different view perspectives.

As we were unfortunately not able to access the specific Colibri II surgical drill model used in collection of the SynColibri benchmark dataset, we created a representative 3D printed surgical drill model of identical geometry to use for qualitative evaluation. Even though our 3D printed model did not have a similar color or texture scheme as the real drill, we were able to demonstrate promising tracking performance using our HMD-EgoPose network. As is visible in the supplementary video material, due to the heavy cropping of input training data to center on the surgical drill, like in Figure 6 (a), our network loses tracking when the drill moves away from the center of the image frame. A future fix for this problem could be to train a lightweight object detection framework like YOLOv4 [63] for prediction of a 2D bounding box around the surgical drill for use in adaptive cropping of input video frames.

Another limitation of this work is with regards to the tracking latency and performance. In our current implementation, we achieved a pixel-to-photon latency of 202.5 ms, resulting in tracking performance of roughly 5 frames per second. We set out to optimize the latency of image frame preprocessing and GPU-based inference; however, the main contributor to latency was the roughly 170 ms that was required for image data transmission from the HoloLens 2 to the computing workstation. With the emerging trend in OST-HMD development favoring the design of lightweight headsets with minimal on-board computing hardware and a cloud-based computing approach to processing, we expect that our contributions to enable a tracking strategy based on low-latency communication with a high-performance computing workstation will be especially valuable. We also expect that the 170 ms required for transmission of video frames from the OST-HMD to the computing workstation could be significantly reduced with future integration of 5G computing, improving the overall pixel-to-photon latency, and furthering the possibility of clinically viable OST-HMD led marker-less surgical instrument tracking.

4 Conclusion

The focus of this work was to contribute to the improvement of egocentric 6DoF object and hand pose estimation strategies from monocular RGB data through further investigating the mutual interactions of the hand of a user and a surgical instrument. With HMD-EgoPose, we demonstrated state-of-the-art performance in hand and surgical drill pose estimation as well as network inference speed through our single-shot pose estimation approach. Further, we showed the feasibility of a low-latency streaming method to enable AR-based egocentric surgical navigation on a commercially available OST-HMD, opening numerous possible avenues for use in surgical tool tracking, 3D to 3D OST-HMD display calibration, and tracking of other rigid landmark objects in the operating room.

Our HMD-EgoPose framework for egocentric surgical tool and hand tracking provides researchers with the means for improved tracking accuracy and robustness to occlusion during challenging 3D tasks in AR-led surgical navigation and, with future developments to the network architecture and training dataset diversity, could contribute to improved patient outcomes. With modifications to the training dataset for the specific intervention, we expect that our modular framework could have significant implications in many other surgical interventions which rely on the tracking of surgical tools or instruments for guidance.

References

- [1] F. Kishino and Milgram, Paul, "A Taxonomy of Mixed Reality Visual Displays," *IEICE Trans. Inf. Syst.*, p. 16, Dec. 1994.
- [2] T. Sielhorst, M. Feuerstein, and N. Navab, "Advanced Medical Displays: A Literature Review of Augmented Reality," *J. Disp. Technol.*, vol. 4, no. 4, pp. 451–467, Dec. 2008, doi: 10.1109/JDT.2008.2001575.
- [3] N. Navab, T. Blum, L. Wang, A. Okur, and T. Wendler, "First Deployments of Augmented Reality in Operating Rooms," *Computer*, vol. 45, no. 7, pp. 48–55, Jul. 2012, doi: 10.1109/MC.2012.75.
- [4] K. Cleary and T. M. Peters, "Image-Guided Interventions: Technology Review and Clinical Applications," *Annu. Rev. Biomed. Eng.*, vol. 12, no. 1, pp. 119–142, Jul. 2010, doi: 10.1146/annurev-bioeng-070909-105249.
- [5] A. Sorriento *et al.*, "Optical and Electromagnetic Tracking Systems for Biomedical Applications: A Critical Review on Potentialities and Limitations," *IEEE Rev. Biomed. Eng.*, vol. 13, pp. 212–232, 2020, doi: 10.1109/RBME.2019.2939091.
- [6] J. Halliday and I. Kamaly, "Use of the Brainlab Disposable Stylet for endoscope and peel-away navigation," *Acta Neurochir. (Wien)*, vol. 158, no. 12, pp. 2327–2331, Dec. 2016, doi: 10.1007/s00701-016-2981-3.
- [7] D. Liu, S. A. Jenkins, P. M. Sanderson, P. Fabian, and W. J. Russell, "Monitoring with Head-Mounted Displays in General Anesthesia: A Clinical Evaluation in the Operating Room," *Anesth. Analg.*, vol. 110, no. 4, pp. 1032–1038, Apr. 2010, doi: 10.1213/ANE.0b013e3181d3e647.

- [8] F. Müller, S. Roner, F. Liebmann, J. M. Spirig, P. Fürnstahl, and M. Farshad, “Augmented reality navigation for spinal pedicle screw instrumentation using intraoperative 3D imaging,” *Spine J.*, vol. 20, no. 4, pp. 621–628, Apr. 2020, doi: 10.1016/j.spinee.2019.10.012.
- [9] L. Qian, A. Deguet, and P. Kazanzides, “ARssist: augmented reality on a head-mounted display for the first assistant in robotic surgery,” *Healthc. Technol. Lett.*, vol. 5, no. 5, pp. 194–200, 2018, doi: 10.1049/htl.2018.5065.
- [10] M. Doughty, K. Singh, and N. R. Ghugre, “SurgeonAssist-Net: Towards Context-Aware Head-Mounted Display-Based Augmented Reality for Surgical Guidance,” in *Medical Image Computing and Computer Assisted Intervention – MICCAI 2021*, Cham, 2021, pp. 667–677. doi: 10.1007/978-3-030-87202-1_64.
- [11] S. Bernhardt, S. A. Nicolau, L. Soler, and C. Doignon, “The status of augmented reality in laparoscopic surgery as of 2016,” *Med. Image Anal.*, vol. 37, pp. 66–90, Apr. 2017, doi: 10.1016/j.media.2017.01.007.
- [12] A. Meola, F. Cutolo, M. Carbone, F. Cagnazzo, M. Ferrari, and V. Ferrari, “Augmented reality in neurosurgery: a systematic review,” *Neurosurg. Rev.*, vol. 40, no. 4, pp. 537–548, Oct. 2017, doi: 10.1007/s10143-016-0732-9.
- [13] L. Jud *et al.*, “Applicability of augmented reality in orthopedic surgery – A systematic review,” *BMC Musculoskelet. Disord.*, vol. 21, no. 1, p. 103, Feb. 2020, doi: 10.1186/s12891-020-3110-2.
- [14] M. Doughty and N. R. Ghugre, “Head-Mounted Display-Based Augmented Reality for Image-Guided Media Delivery to the Heart: A Preliminary Investigation of Perceptual Accuracy,” *J. Imaging*, vol. 8, no. 2, Art. no. 2, Feb. 2022, doi: 10.3390/jimaging8020033.
- [15] R. Rahman, M. E. Wood, L. Qian, C. L. Price, A. A. Johnson, and G. M. Osgood, “Head-Mounted Display Use in Surgery: A Systematic Review,” *Surg. Innov.*, vol. 27, no. 1, pp. 88–100, Feb. 2020, doi: 10.1177/1553350619871787.
- [16] J. M. Fitzpatrick, “The Role of Registration in Accurate Surgical Guidance,” *Proc. Inst. Mech. Eng. [HJ]*, vol. 224, no. 5, pp. 607–622, 2010.
- [17] V. Lahanas, C. Loukas, and E. Georgiou, “A simple sensor calibration technique for estimating the 3D pose of endoscopic instruments,” *Surg. Endosc.*, vol. 30, no. 3, pp. 1198–1204, Mar. 2016, doi: 10.1007/s00464-015-4330-7.
- [18] R. Elfring, M. de la Fuente, and K. Radermacher, “Assessment of optical localizer accuracy for computer aided surgery systems,” *Comput. Aided Surg.*, vol. 15, no. 1–3, pp. 1–12, 2010, doi: 10.3109/10929081003647239.
- [19] F. Liebmann *et al.*, “Registration made easy -- standalone orthopedic navigation with HoloLens,” *ArXiv200106209 Cs*, Jan. 2020, Accessed: May 27, 2020. [Online]. Available: <http://arxiv.org/abs/2001.06209>
- [20] E. Azimi, L. Qian, N. Navab, and P. Kazanzides, “Alignment of the Virtual Scene to the Tracking Space of a Mixed Reality Head-Mounted Display,” *ArXiv170305834 Cs*, Mar. 2019, Accessed: May 27, 2020. [Online]. Available: <http://arxiv.org/abs/1703.05834>
- [21] F. Poulin and L.-P. Amiot, “Interference during the use of an electromagnetic tracking system under OR conditions,” *J. Biomech.*, vol. 35, no. 6, pp. 733–737, Jun. 2002, doi: 10.1016/S0021-9290(02)00036-2.
- [22] A. Krizhevsky, I. Sutskever, and G. E. Hinton, “ImageNet Classification with Deep Convolutional Neural Networks,” in *Advances in Neural Information Processing Systems 25*, F. Pereira, C. J. C. Burges, L. Bottou, and K. Q. Weinberger, Eds. Curran Associates, Inc.,

- 2012, pp. 1097–1105. Accessed: Jun. 16, 2020. [Online]. Available: <http://papers.nips.cc/paper/4824-imagenet-classification-with-deep-convolutional-neural-networks.pdf>
- [23] J. Redmon and A. Farhadi, “YOLO9000: Better, Faster, Stronger,” in *2017 IEEE Conference on Computer Vision and Pattern Recognition (CVPR)*, Honolulu, HI, Jul. 2017, pp. 6517–6525. doi: 10.1109/CVPR.2017.690.
- [24] Y. Xiang, T. Schmidt, V. Narayanan, and D. Fox, “PoseCNN: A Convolutional Neural Network for 6D Object Pose Estimation in Cluttered Scenes,” *ArXiv171100199 Cs*, May 2018, Accessed: Jan. 06, 2022. [Online]. Available: <http://arxiv.org/abs/1711.00199>
- [25] C. Sahin and T.-K. Kim, “Recovering 6D Object Pose: A Review and Multi-modal Analysis,” in *Computer Vision – ECCV 2018 Workshops*, vol. 11134, L. Leal-Taixé and S. Roth, Eds. Cham: Springer International Publishing, 2019, pp. 15–31. doi: 10.1007/978-3-030-11024-6_2.
- [26] S. Hinterstoisser *et al.*, “Model Based Training, Detection and Pose Estimation of Texture-Less 3D Objects in Heavily Cluttered Scenes,” in *Computer Vision – ACCV 2012*, vol. 7724, K. M. Lee, Y. Matsushita, J. M. Rehg, and Z. Hu, Eds. Berlin, Heidelberg: Springer Berlin Heidelberg, 2013, pp. 548–562. doi: 10.1007/978-3-642-37331-2_42.
- [27] B. Drost, M. Ulrich, N. Navab, and S. Ilic, “Model globally, match locally: Efficient and robust 3D object recognition,” in *2010 IEEE Computer Society Conference on Computer Vision and Pattern Recognition*, Jun. 2010, pp. 998–1005. doi: 10.1109/CVPR.2010.5540108.
- [28] A. Tejani, D. Tang, R. Kouskouridas, and T.-K. Kim, “Latent-Class Hough Forests for 3D Object Detection and Pose Estimation,” in *Computer Vision – ECCV 2014*, Cham, 2014, pp. 462–477. doi: 10.1007/978-3-319-10599-4_30.
- [29] E. Brachmann, A. Krull, F. Michel, S. Gumhold, J. Shotton, and C. Rother, “Learning 6D Object Pose Estimation Using 3D Object Coordinates,” in *Computer Vision – ECCV 2014*, Cham, 2014, pp. 536–551. doi: 10.1007/978-3-319-10605-2_35.
- [30] F. Michel *et al.*, “Global Hypothesis Generation for 6D Object Pose Estimation,” in *2017 IEEE Conference on Computer Vision and Pattern Recognition (CVPR)*, Honolulu, HI, Jul. 2017, pp. 115–124. doi: 10.1109/CVPR.2017.20.
- [31] W. Kehl, F. Milletari, F. Tombari, S. Ilic, and N. Navab, “Deep Learning of Local RGB-D Patches for 3D Object Detection and 6D Pose Estimation,” in *Computer Vision – ECCV 2016*, Cham, 2016, pp. 205–220. doi: 10.1007/978-3-319-46487-9_13.
- [32] Y. He, W. Sun, H. Huang, J. Liu, H. Fan, and J. Sun, “PVN3D: A Deep Point-Wise 3D Keypoints Voting Network for 6DoF Pose Estimation,” in *2020 IEEE/CVF Conference on Computer Vision and Pattern Recognition (CVPR)*, Seattle, WA, USA, Jun. 2020, pp. 11629–11638. doi: 10.1109/CVPR42600.2020.01165.
- [33] F. Mueller, D. Mehta, O. Sotnychenko, S. Sridhar, D. Casas, and C. Theobalt, “Real-Time Hand Tracking Under Occlusion From an Egocentric RGB-D Sensor,” p. 10.
- [34] J. Hein *et al.*, “Towards markerless surgical tool and hand pose estimation,” *Int. J. Comput. Assist. Radiol. Surg.*, Apr. 2021, doi: 10.1007/s11548-021-02369-2.
- [35] B. Tekin, S. N. Sinha, and P. Fua, “Real-Time Seamless Single Shot 6D Object Pose Prediction,” in *2018 IEEE/CVF Conference on Computer Vision and Pattern Recognition*, Jun. 2018, pp. 292–301. doi: 10.1109/CVPR.2018.00038.

- [36] Y. Bukschat and M. Vetter, “EfficientPose: An efficient, accurate and scalable end-to-end 6D multi object pose estimation approach,” *ArXiv201104307 Cs*, Nov. 2020, Accessed: Jan. 05, 2022. [Online]. Available: <http://arxiv.org/abs/2011.04307>
- [37] A. Kendall, M. Grimes, and R. Cipolla, “PoseNet: A Convolutional Network for Real-Time 6-DOF Camera Relocalization,” in *2015 IEEE International Conference on Computer Vision (ICCV)*, Santiago, Chile, Dec. 2015, pp. 2938–2946. doi: 10.1109/ICCV.2015.336.
- [38] S. Zakharov, I. Shugurov, and S. Ilic, “DPOD: 6D Pose Object Detector and Refiner,” in *2019 IEEE/CVF International Conference on Computer Vision (ICCV)*, Seoul, Korea (South), Oct. 2019, pp. 1941–1950. doi: 10.1109/ICCV.2019.00203.
- [39] S. Peng, Y. Liu, Q. Huang, X. Zhou, and H. Bao, “PVNet: Pixel-Wise Voting Network for 6DoF Pose Estimation,” in *2019 IEEE/CVF Conference on Computer Vision and Pattern Recognition (CVPR)*, Long Beach, CA, USA, Jun. 2019, pp. 4556–4565. doi: 10.1109/CVPR.2019.00469.
- [40] C. Song, J. Song, and Q. Huang, “HybridPose: 6D Object Pose Estimation Under Hybrid Representations,” in *2020 IEEE/CVF Conference on Computer Vision and Pattern Recognition (CVPR)*, Seattle, WA, USA, Jun. 2020, pp. 428–437. doi: 10.1109/CVPR42600.2020.00051.
- [41] M. Rad and V. Lepetit, “BB8: A Scalable, Accurate, Robust to Partial Occlusion Method for Predicting the 3D Poses of Challenging Objects without Using Depth,” in *2017 IEEE International Conference on Computer Vision (ICCV)*, Venice, Oct. 2017, pp. 3848–3856. doi: 10.1109/ICCV.2017.413.
- [42] K. Park, T. Patten, and M. Vincze, “Pix2Pose: Pixel-Wise Coordinate Regression of Objects for 6D Pose Estimation,” in *2019 IEEE/CVF International Conference on Computer Vision (ICCV)*, Seoul, Korea (South), Oct. 2019, pp. 7667–7676. doi: 10.1109/ICCV.2019.00776.
- [43] M. A. Fischler and R. C. Bolles, “Random Sample Consensus: A Paradigm for Model Fitting with Applications to Image Analysis and Automated Cartography,” *Commun. ACM*, vol. 24(6), no. 381–395, p. 42, 1981.
- [44] V. Athitsos and S. Sclaroff, “Estimating 3D hand pose from a cluttered image,” in *2003 IEEE Computer Society Conference on Computer Vision and Pattern Recognition, 2003. Proceedings.*, Jun. 2003, vol. 2, p. II–432. doi: 10.1109/CVPR.2003.1211500.
- [45] B. Stenger, P. R. S. Mendonca, and R. Cipolla, “Model-based 3D tracking of an articulated hand,” in *Proceedings of the 2001 IEEE Computer Society Conference on Computer Vision and Pattern Recognition. CVPR 2001*, Dec. 2001, vol. 2, p. II–II. doi: 10.1109/CVPR.2001.990976.
- [46] L. Yang and A. Yao, “Disentangling Latent Hands for Image Synthesis and Pose Estimation,” in *2019 IEEE/CVF Conference on Computer Vision and Pattern Recognition (CVPR)*, Long Beach, CA, USA, Jun. 2019, pp. 9869–9878. doi: 10.1109/CVPR.2019.01011.
- [47] Y. Cai, L. Ge, J. Cai, and J. Yuan, “Weakly-Supervised 3D Hand Pose Estimation from Monocular RGB Images,” in *Computer Vision – ECCV 2018*, vol. 11210, V. Ferrari, M. Hebert, C. Sminchisescu, and Y. Weiss, Eds. Cham: Springer International Publishing, 2018, pp. 678–694. doi: 10.1007/978-3-030-01231-1_41.

- [48] U. Iqbal, P. Molchanov, T. Breuel, J. Gall, and J. Kautz, "Hand Pose Estimation via Latent 2.5D Heatmap Regression," in *Computer Vision – ECCV 2018*, vol. 11215, V. Ferrari, M. Hebert, C. Sminchisescu, and Y. Weiss, Eds. Cham: Springer International Publishing, 2018, pp. 125–143. doi: 10.1007/978-3-030-01252-6_8.
- [49] F. Mueller *et al.*, "GANerated Hands for Real-Time 3D Hand Tracking from Monocular RGB," in *2018 IEEE/CVF Conference on Computer Vision and Pattern Recognition*, Salt Lake City, UT, Jun. 2018, pp. 49–59. doi: 10.1109/CVPR.2018.00013.
- [50] A. Spurr, J. Song, S. Park, and O. Hilliges, "Cross-Modal Deep Variational Hand Pose Estimation," in *2018 IEEE/CVF Conference on Computer Vision and Pattern Recognition*, Salt Lake City, UT, Jun. 2018, pp. 89–98. doi: 10.1109/CVPR.2018.00017.
- [51] J. Romero, D. Tzionas, and M. J. Black, "Embodied hands: modeling and capturing hands and bodies together," *ACM Trans. Graph.*, vol. 36, no. 6, pp. 1–17, Nov. 2017, doi: 10.1145/3130800.3130883.
- [52] H. Joo, T. Simon, and Y. Sheikh, "Total Capture: A 3D Deformation Model for Tracking Faces, Hands, and Bodies," in *2018 IEEE/CVF Conference on Computer Vision and Pattern Recognition*, Salt Lake City, UT, USA, Jun. 2018, pp. 8320–8329. doi: 10.1109/CVPR.2018.00868.
- [53] Y. Hasson *et al.*, "Learning Joint Reconstruction of Hands and Manipulated Objects," in *2019 IEEE/CVF Conference on Computer Vision and Pattern Recognition (CVPR)*, Long Beach, CA, USA, Jun. 2019, pp. 11799–11808. doi: 10.1109/CVPR.2019.01208.
- [54] Y. Hasson, B. Tekin, F. Bogo, I. Laptev, M. Pollefeys, and C. Schmid, "Leveraging Photometric Consistency Over Time for Sparsely Supervised Hand-Object Reconstruction," in *2020 IEEE/CVF Conference on Computer Vision and Pattern Recognition (CVPR)*, Seattle, WA, USA, Jun. 2020, pp. 568–577. doi: 10.1109/CVPR42600.2020.00065.
- [55] M. Tan, R. Pang, and Q. V. Le, "EfficientDet: Scalable and Efficient Object Detection," in *2020 IEEE/CVF Conference on Computer Vision and Pattern Recognition (CVPR)*, Seattle, WA, USA, Jun. 2020, pp. 10778–10787. doi: 10.1109/CVPR42600.2020.01079.
- [56] M. Tan and Q. Le, "EfficientNet: Rethinking Model Scaling for Convolutional Neural Networks," in *Proceedings of the 36th International Conference on Machine Learning*, May 2019, pp. 6105–6114. Accessed: Jan. 10, 2022. [Online]. Available: <https://proceedings.mlr.press/v97/tan19a.html>
- [57] A. Paszke *et al.*, "PyTorch: An Imperative Style, High-Performance Deep Learning Library," in *Advances in Neural Information Processing Systems*, 2019, vol. 32. Accessed: Jan. 11, 2022. [Online]. Available: <https://proceedings.neurips.cc/paper/2019/hash/bdbca288fee7f92f2bfa9f7012727740-Abstract.html>
- [58] D. P. Kingma and J. Ba, "Adam: A Method for Stochastic Optimization," *ArXiv14126980 Cs*, Jan. 2017, Accessed: Apr. 21, 2020. [Online]. Available: <http://arxiv.org/abs/1412.6980>
- [59] Z. Zhang, "A flexible new technique for camera calibration," *IEEE Trans. Pattern Anal. Mach. Intell.*, vol. 22, no. 11, pp. 1330–1334, Nov. 2000, doi: 10.1109/34.888718.
- [60] O. Ronneberger, P. Fischer, and T. Brox, "U-Net: Convolutional Networks for Biomedical Image Segmentation," in *Medical Image Computing and Computer-Assisted Intervention – MICCAI 2015*, Cham, 2015, pp. 234–241.

- [61] K. He, X. Zhang, S. Ren, and J. Sun, “Deep Residual Learning for Image Recognition,” *ArXiv151203385 Cs*, Dec. 2015, Accessed: Apr. 27, 2020. [Online]. Available: <http://arxiv.org/abs/1512.03385>
- [62] A. Bochkovskiy, C.-Y. Wang, and H.-Y. M. Liao, “YOLOv4: Optimal Speed and Accuracy of Object Detection,” *ArXiv200410934 Cs Eess*, Apr. 2020, Accessed: May 01, 2020. [Online]. Available: <http://arxiv.org/abs/2004.10934>